Journal of Materials Chemistry A

Accepted Manuscript

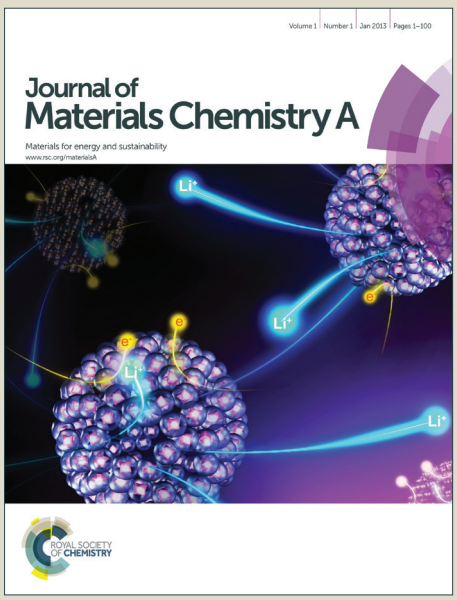

ROYAL SOCIETY OF CHEMISTRY

www.rsc.org/materialsA

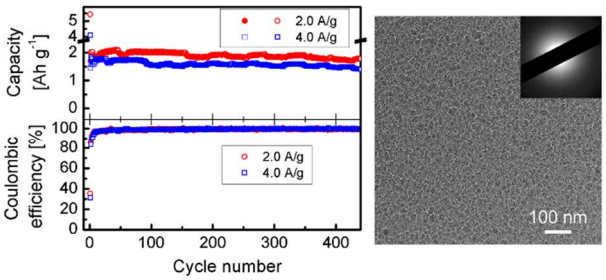

One step plasma deposited Si/C nanocomposites as high capacity, high stability lithium ion battery anodes.

Journal Name

RSCPublishing

ARTICLE

Direct plasma deposition of amorphous Si/C nanocomposites as high performance anode for lithium ion batteries

Cite this: DOI: 10.1039/x0xx00000x

Received 00th January 2012,
Accepted 00th January 2012

DOI: 10.1039/x0xx00000x

www.rsc.org/

Xinghua Chang,[a,b] Wei Li,[c] Junfeng Yang,[a] Li Xu,[d] Jie Zheng[a]* and Xingguo Li[a]*

Plasma reactions are very effective in preparation of both silicon and carbon materials. However, Si/C composites, which are highly attractive as the anode material in lithium ion batteries, are difficult to be prepared using plasma due to the strong tendency of silicon carbide (SiC) formation. Here we effectively inhibit the SiC formation by generating reactive Si and C species in separated plasma zones and by using a solid graphite carbon precursor. Homogeneous Si/C nanocomposites with excellent lithium storage performance are obtained from one step plasma deposition at room temperature, which retain high capacity of 1760 and 1460 mAh·g^{-1} after more than 400 cycles at charge/discharge rate of 2.0 and 4.0 A·g^{-1}, respectively.

Introduction

Developing electrode materials with high capacity and long cycle stability is of critical importance to further enhance the performance of lithium ion batteries (LIBs). Silicon is highly attractive as the anode material for LIBs due to its very high theoretical capacity of 4200 mAh·g^{-1}[1], which is about 10 times higher than that of graphite used in current commercial LIBs. However, Si based anodes suffer from poor stability due to the huge volume change during the charge/discharge process[2, 3]. Si based thin film structures exhibit higher tolerance to the change/discharge induced stress and thus have shown promising application as the LIB anode[4]. Takamura et al[5] and Chen et al[6] have reported high reversible capacity and good capacity retention for amorphous Si thin films. However, rapid capacity fading is frequently observed for pure Si films with thickness of several hundred nanometers[7-9]. Patterned silicon thin films with 50-100 μm lateral dimension would relieve the lateral stress and improve the capacity retention[7, 10]. Compared to pure Si thin films, Si based thin films, including partially oxidized silicon thin films[9], silicon nitride[8, 11] thin films or multilayer thin films with Ti[12] or carbon[13-15] interlayers generally exhibit better capacity retention.

An important strategy to overcome the volume change induced structural instability is to introduce carbon as a structure buffer and a conductive matrix. This strategy has been widely employed for alloy type anodes in LIBs[16, 17] and is very promising to enhance the cyclic stability of Si[18-28]. Currently there are two major strategies to prepare Si/C nanocomposites. Post synthetic carbon modification of silicon nanoparticles is most commonly applied[19-24]. This approach is advanced by surface engineering to allow more homogeneous coating of the carbon materials[23, 24]. However, it is also limited by the availability of high quality silicon nanostructures. Another approach is depositing silicon onto existing carbon nanostructures, typically by thermal or plasma decomposition of SiH_4[26-28]. This approach can utilize the large variety of carbon nanostructures available. However, homogeneous loading of Si onto the carbon substrates is difficult, particularly when the carbon substrates contain space that is difficult to access. Recently, some researchers also prepared Si/C composites from thermal reduction of silicon compounds by reactive metal in organic solvents [29] or solid state [30]. Despite of their success in obtaining Si/C composites with decent lithium storage performance, the above methods require sophisticated, multistep processes.

Plasma reactions, such as plasma enhanced chemical vapour deposition, sputtering and laser ablation, are highly efficient in preparing both silicon and carbon nanostructures from simple molecular or solid precursors[31]. Preparation of Si/C composites plasma reaction seems quite promising by simply introducing both the Si and C precursors into plasma. However, in this case SiC instead of Si/C composites is more inclined to form, due to the strong bonding tendency between Si and C[32, 33]. Recently, Hu et al developed a plasma assisted ball milling process, which efficiently converted the natural graphite into graphene layers coating on the Si nanoparticles without SiC formation[34, 35]. Except for this non-typical plasma reaction, one step preparation of Si/C nanocomposites without SiC formation remains difficult.

Recently we have developed a general approach for controlled preparation of carbon based binary composites based on a tandem plasma reaction (TPR)[13, 36, 37]. The TPR integrates

two plasma sources in one reactor: a magnetron sputtering source for metal cluster generation and an inductively coupled plasma (ICP) source for carbon incorporation, respectively. This configuration allows to generate the two components in a binary composite in two separated plasma zones, which offers the possibility to inhibit compound formation between two components with strong interaction. However, the recently work by Chaukulkar et al[38] in a similar two zone plasma reactor shows that there remained notable SiC formation even if the two plasma zones for Si formation and carbon coating were separated.

In this paper, we demonstrate that by using graphite as the carbon precursor in the TPR, formation of SiC can be effectively inhibited. Homogeneous Si/C nanocomposite can be directly obtained in one step, which exhibits excellent performance as the anode of LIBs, with high reversible capacity of 2100 $mAh{\cdot}g^{-1}$ after 200 cycles at current density of 0.40 $A{\cdot}g^{-1}$ and 1460 $mAh{\cdot}g^{-1}$ after 400 cycles at current density of 4.0 $A{\cdot}g^{-1}$.

Experimental

Setups and experimental details

The tendem plasma reactor (TPR) used to prepare the Si/C nanocomposites is schematically illustrated in Figure 1, which is composed of a magnetron sputtering source an inductively couple plasma (ICP) coil between the target and the substrate. The distance between the target and the substrate is 15 cm. The ICP coil is located 2 cm above the substrate. The chamber is first evacuated to 8×10^{-4} Pa by a diffusion pump. Si particles are generated by magnetron sputtering of a high purity Si target (>99.9995%) using high purity argon (99.995%) with flow rate of 20.0 sccm (Standard Cubic Centimeter per Second). During deposition, the chamber pressure is maintained at 5.0 Pa. The power of both the magnetron sputtering and ICP is 100 W. The composites are deposited without heating the substrates. The effect of plasma causes a slight increase of the substrate temperature to about 50 °C in the deposition conditions.

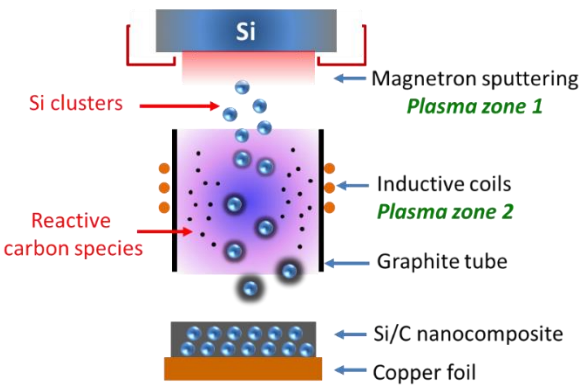

Figure 1 Schematic illustration of the tandem plasma reactor (TPR) for preparation of Si/C nanocomposites

Carbon is generated in the ICP zone by either decomposition of CH_4 or sputtering of a graphite surface. When CH_4 is used as the carbon precursor, CH_4 (99.95%) is inlet in a separate gas line into the ICP zone with a low flow rate of 1.0 sccm. The sample obtained is denoted as Si/C-CH_4. When graphite is used as the carbon precursor, a graphite tube made from rolling of a high purity graphite sheet with thickness of 1 mm is mounted inside the ICP coil. Only Ar is used in this case with flow rate of 20 sccm. The sample obtained is denoted as Si/C-graphite.

Structural characterization

The structure of the composites is characterized by scanning electron microscopy (SEM, Hitachi S4800, 10 kV) with an energy dispersive X-ray spectroscopy (EDS) analyzer, transmission electron microscopy (TEM, JEOL JEM-2100, 200 kV), atomic force microscopy (AFM, Seiko SPA-400) and X-ray photoelectron spectroscopy (XPS, Kratos Analytical, Ultra Axis). The composition of the components is determined by energy dispersed spectroscopy (EDS) in SEM and XPS for samples deposited on copper foils. To eliminate the surface carbon contaminant in XPS measurement, the surface of the sample is first cleaning by Ar^+ beam sputtering. The results obtained by the two methods are in good agreement with each other. For AFM measurement, the sample is deposited on a Si (001) wafer with a 100 nm oxide layer. For TEM measurement, the samples deposited on copper foils are transferred onto the TEM grid. The sample surface is first gently scratched with a sharp blade and is subsequently sonicated in absolute ethanol for 10 min. Several drops of the suspension is casted onto the TEM grid.

Electrochemical measurement

The electrodes used in electrochemical performance measurements are fabricated by direct deposition of the sample on copper foils. The mass loading (50-100 $\mu g{\cdot}cm^{-2}$) is determined by a high accuracy microbalance (Mettler Toledo, accuracy 1 μg) and also calculated from the deposition rate. Coin type half-cells were assembled in an argon-filled glove-box. A lithium foil was utilized as the counter electrode. 1 M $LiPF_6$ in ethylene carbonate/dimethyl carbonate = 1/1 in volume was used as the electrolyte. Polypropylene films (Celgard 2400) were used as the separators. The cells were tested at current density from 400 to 4000 $mA{\cdot}g^{-1}$ for both charge and discharge at room temperature in the voltage range of 0.005 – 2.0 V (versus Li/Li^+). Cyclic voltammetric measurements were performed in the voltage range of 2.5 - 0 V (versus Li/Li^+) at a scan rate of 0.1 $mV{\cdot}s^{-1}$.

Results and Discussions

The structural characterization of the Si/C-graphite sample is shown in Figure 2. The TEM image (Figure 2a) suggests that the nanocomposite is composed of homogeneously distributed nanoparticles around 20 nm in size. The electron diffraction pattern (Figure 2a, inset) only shows a very diffused ring, indicating that the nanocomposite is amorphous. As shown by the AFM result (Figure 2b and 2c), the surface is very smooth, with root mean square (RMS) roughness of only 0.6 nm. This is in agreement with the cross section SEM image (Figure S1). Elemental analysis (Figure S2) suggests that the nanocomposite is composed of Si and C. As shown by the 2D elemental mapping (Figure 2d-2f), the two elements are distributed very homogeneously across the substrate. The Si/C-CH_4 sample exhibits very similar structural features in terms of the composition, the distribution of the two components and the crystallinity (Figure S3, S4). The carbon fraction in the composite can be controlled by either the power of the two plasma sources (Figure S5) or the CH_4 fraction for the Si/C-CH4 samples. In this study, the carbon fraction is kept at 10 wt% for both the Si/C-graphite and Si/C-CH_4 samples.

Despite of many structural similarities, the two Si/C samples exhibit distinct chemical bonding states of Si, which is suggested by the XPS spectra (Figure 3a). The dominate peak of the Si/C-graphite sample is located at 99.3 eV, which is corresponding to the elemental Si[39, 40]. There is a low shoulder peak at 103 eV corresponding to partially oxidized silicon[25], which is formed when exposed to air during the transferring. Therefore, the Si/C-graphite nanocomposite is composed of elemental Si and C. For the Si/C-CH_4 sample, the Si 2p peak is shifted to 101.2 eV, which matches that of silicon carbide[39, 40]. There should be still considerable elemental Si, as the composite only contains 10 wt% carbon (21 at%). However, the XPS spectrum suggests the contribution from elemental Si is very weak. As XPS is surface sensitive, the above results imply that the elemental Si must be finely covered by the formed carbide. This is also in agreement with the reaction picture of TPR, in which Si nanoclusters are first generated by magnetron sputtering and are subsequently coated by carbon in the ICP zone.

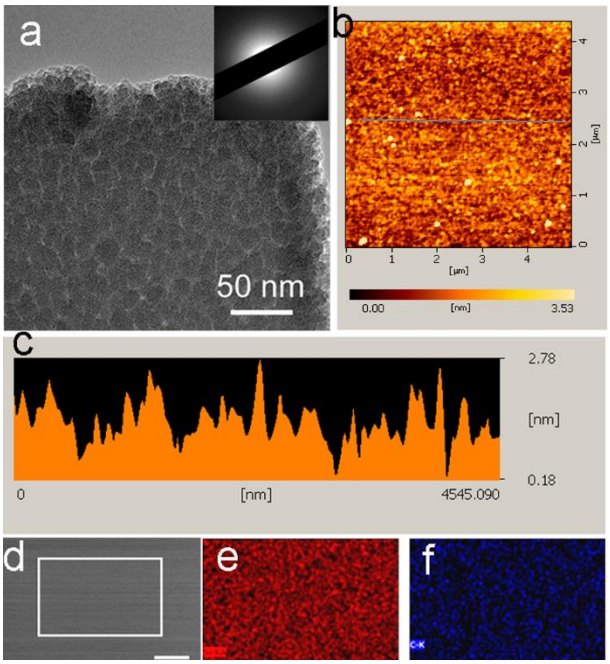

Figure 2 Characterization of the Si/C-graphite sample (a) A TEM image. The inset is a selected area electron diffraction pattern. (b) AFM mapping, (c) Height profile scanning along the line indicated in (b), (d) SEM image (scale bar = 2 μm), (e) Si mapping and (f) C mapping of the rectangular area in (d).

In our previous study, Sn/C and Ge/C nanocomposites can be directly obtained by TPR using CH_4 as the carbon precursor[36, 37]. Compared to Sn and Ge, Si exhibits much stronger tendency to form carbide. Theoretical studies suggest that the formation enthalpy is negative for SiC while positive for GeC and SnC at ambient pressure and temperature, becoming more positive in the order of SiC < GeC < SnC[41]. As will be shown later, SiC formation is very detrimental for the lithium storage application (Figure 4b) and should be minimized. However, the plasma condition seems too reactive to prevent the SiC formation. Previous experimental study suggests that SiC can be readily obtained in plasma reactions when reactive Si and C species are in direct contact[32, 33]. In TPR, although the two reactive species are generated in two plasma zones, carbide is still formed when CH_4 is used as the carbon precursor. On the other hand, when graphite is used instead of CH_4, the carbide formation is effectively suppressed.

To understand the effect of different carbon precursors, optical emission spectra (OES) of the plasma during the deposition is collected. The emission peaks corresponding to atomic Si at 251 and 288 nm[42, 43] are very weak (Figure S6), which suggests that the majority of the Si species generated by sputtering should be in the form of clusters instead of isolated atoms. This is in agreement with previous study on magnetron sputtering of Si[44]. When CH_4 is used, the emission bands corresponding to CH (431 nm), C_2 (455-475 nm, 516 nm) and atomic H (486 nm, the H_β line) can be identified (Figure 3b). The CH group and the atomic H are generated from dissociation of CH_4. The C_2 group is extensively observed in plasmas containing hydrocarbon molecules, which is generated from further reaction of the reactive carbon species[45, 46]. When graphite is used, the only notable carbon containing reactive species is the C_2 group. Weak emission from the hydrogen containing species (CH and H) is also observed in this case, which is from the sputtering of the hydrogenated amorphous carbon deposited in the chamber in precedent experiments. In fact, the idea of using a solid carbon precursor is first conceived from this contamination phenomenon. We have noticed that when the reactor was not frequently cleaned, some "pure Si" samples deposited without CH_4 also contained appreciable fraction of carbon and exhibited better electrode performance than the pure Si, which prompted us to use a solid carbon precursor intentionally.

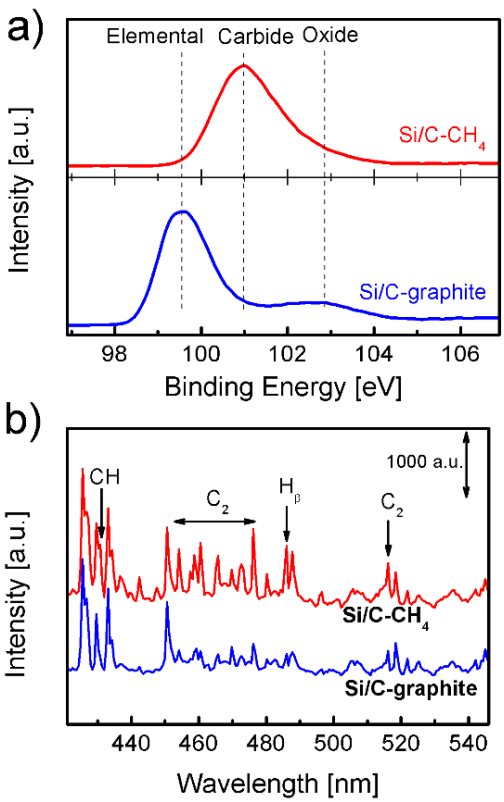

Figure 3 (a) Si 2p X-ray photoelectron spectra and (b) The optical emission spectra collected in situ during the preparation process of the Si/C-CH_4 and Si/C-graphite samples. The intensity of the spectra are normalized with respect to the atomic Ar line at 867 nm.

The absolute intensity of the emission lines is subjected to a number of factors and cannot be directly compared. We normalize the intensity of the spectra with respect to the Ar emission line at 867 nm. Clearly, the intensity of the peaks related to the reactive carbon species (C_2 and CH) are much lower when graphite is used as the carbon precursor, indicating that replacing a molecular carbon source (CH_4) with a solid one (graphite) effectively reduces the density of the reactive carbon species. This is further confirmed by the different carbon deposition rate. With 100 W ICP power, the carbon deposition rate is 3.2 nm·min^{-1} for dissociation of CH_4 and only 0.3 nm·min^{-1} for sputtering of graphite. This difference can be understood by the different mechanism in generating the reactive carbon species. The CH_4 molecules can be excited by a number of channels in plasma to generate reactive carbon species, including direct electron impact and energy transfer from other excited species (such as Ar in the excited states or atomic H). On the other hand, sputtering of the graphite surface requires bombardment of Ar^+ with sufficient energy. As the plasma in the ICP region is very dispersed, the density of such high energy cations is very low. Therefore, when replacing CH_4 by graphite, the density of the active carbon species is significantly reduced, which suppresses carbide formation.

Here it is illustrative to compare with the recent work by Chaukulkar et al[38], who prepared carbon coated Si nanoparticles in a similar tandem plasma reactor. Si nanoparticles were generated in the first plasma zone by decomposition of SiH_4 and were coated by carbon in the second plasma zone by decomposition of C_2H_2. According to our above analysis, the gaseous carbon precursor C_2H_2 is too reactive to prevent SiC formation. Indeed, XPS analysis suggested more than 30% of Si is in the form of SiC in their samples, though the two plasma zones were kept away from each other.

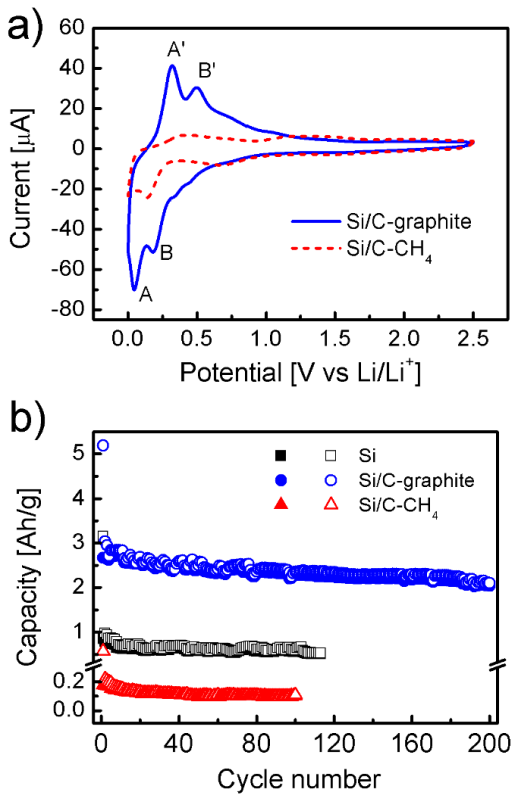

Figure 4 (a) The cyclic voltammetry curves (the 5th cycle) of the Si/C-graphite and Si/C-CH_4 samples. (b) The capacity (based on all the materials on the current collector) in repeated charge/discharge cycles for the pure Si, Si/C-graphite and Si/C-CH_4 samples at current density of 0.40 A·g^{-1}. Both samples contain 10 wt% carbon.

The two Si/C samples from different carbon precursors exhibit different lithiation/delithiation behaviours, as shown by the cyclic voltammetry results of two Si/C samples both containing 10 wt% carbon (Figure 4a). For the Si/C-graphite sample, peaks corresponding to stepwise reactions with lithium can be clearly resolved. The B-B' and A-A' pairs of peaks are corresponding to the reversible lithiation/delithiation reaction of Si[19, 24]. For the Si/C-CH_4 sample, the lithiation/delithiation features become very weak in the CV curve, with only the very weak B peak discernible. The structural characterization suggests that the Si/C-CH_4 sample contains considerable amount of SiC. The CV results suggest that SiC is inactive to lithiation. The remaining weak features in the CV curve are resulted from the residue elemental Si.

Figure 4b compares the lithium storage capacity during repeated charge/discharge cycles of the pure Si sample and two Si/C samples. The first cycle shows extraordinarily high capacity for all the samples, which is mainly attributed to the formation of the solid electrolyte interface (SEI) layer. Formation of the SEI layer is also evidenced by the large difference of in the CV curves for the 1st cycle and the following cycles (Figure S7 and S8). In addition to SEI formation, some partially oxidized Si (as evidenced in Figure 3a) will also contribute to the initial irreversible capacity. For thin film electrodes, this contribution becomes more significant as the amount of the active material is lower. Therefore, the initial Columbic efficiency of the Si/C-graphite sample is lower compared to the typical value of powder Si samples (60-90%)[23-27].

For the pure Si sample, the capacity of the 2nd cycle is only 980 mAh/g and decreases to only 590 mAh/g after 120 cycles. The capacity is much lower than the theoretical value of Si even in the first a few cycles. This indicates that a large fraction of Si is not utilized, which can be attributed to the poor Li^+ conductivity in the dense Si film. The Si/C-graphite sample, on the other hand, exhibits both very high capacity and very good stability (also shown by the capacity-voltage curve in Figure S9). The capacity of the 2nd cycle reaches 3032 mAh·g^{-1}. By correction for the Si content (90 wt%), the contribution from Si to the capacity reaches 3368 mAh·g^{-1}, 80% of the theoretical value of Si. Considering some oxidation of silicon (Figure 3a), the utilization of Si should be even higher. The capacity retention is also significantly improved. After 200 cycles, there remains a high capacity of 2100 mAh·g^{-1}. The Si/C-CH_4 sample, on the other hand, barely shows any lithium storage capacity, which is even much lower than that of the pure Si sample. This is in agreement with the CV results that SiC is inactive to lithiation. Previous study on the lithiation of SiC films implied similar low capacity[47]. Moreover, when the remaining Si is blocked by the inactive SiC phase, the lithiation reaction becomes much more difficult. Therefore, SiC formation also causes significant capacity degradation of the remaining Si.

Clearly, carbon incorporation, though only 10 wt%, significantly improves both the cyclic stability and the Si utilization. The stabilization effect is confirmed by the SEM

images of the electrode after cycles (Figure 5). The pure Si sample exhibits clear cracks, while the Si/C-graphite sample remains intact, with only coarsening of the particles. Although the stabilization effect of carbon for alloy type anode materials is well known, achieving good stabilization effect with minimum amount of carbon is very challenging. In the TPR method, carbon is introduced before the Si clusters reach the substrate, yielding Si/C nanocomposites with very homogenous distribution of the two components (Figure 2d-2f), which is highly favourable to maximize the stabilization effect of carbon. In addition to the stabilization effect, the homogeneously incorporated carbon also facilitates fast Li^+ transport. The diffusion coefficient of Li^+ in carbon is 10^{-11} to 10^{-7} cm^2s^{-1}[48], depending on the nature of the carbon materials and the lithiation degree, which is much higher than that in silicon (10^{-14} to 10^{-12} cm^2s^{-1})[49, 50]. This effect, together with the reduced Si domain size due to carbon incorporation, results in more complete utilization of the active materials even at high current density.

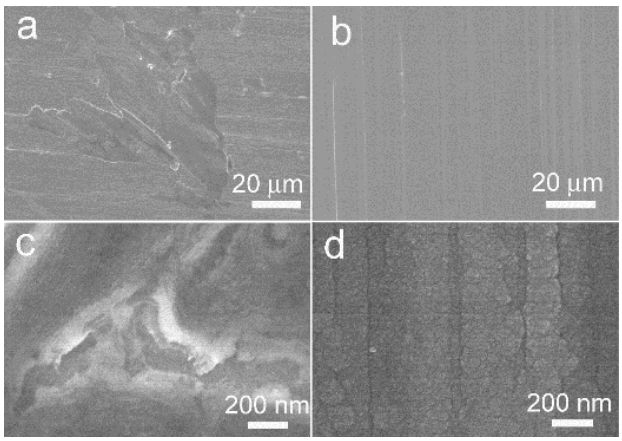

Figure 5 The planar view SEM images of the pure Si (a, c) and the Si/C-graphite sample (b, d) after 100 charge/discharge cycles.

The performance of the Si/C-graphite sample with 10 wt% carbon is further characterized at different charge/discharge current density. As shown in Figure 6a, at a high charging rate of 4.0 $A{\cdot}g^{-1}$, a high capacity of 1020 $mAh{\cdot}g^{-1}$ is still obtained, indicating very good lithiation/delithiation kinetics. When the current density is switched back to 0.40 $A{\cdot}g^{-1}$, the capacity again increases to 2500 $mAh{\cdot}g^{-1}$. Even better performance is obtained when the cells are maintaining at high charge/discharge rate. As shown in Figure 6b, at current density of 2.0 and 4.0 $A{\cdot}g^{-1}$, the capacity remains 1760 and 1460 $mAh{\cdot}g^{-1}$ after more than 400 cycles. The Columbic efficiency rapidly exceeds 95% in the first a few cycles and maintains higher than 99.5% in the steady operation. It should be emphasized that the electrodes prepared by TPR are binder free. The capacity shown in Figure 6 is based on all the materials on the current collector.

Even considering that thin film electrodes usually exhibit better cyclic stability due to the stress relaxation in the direction perpendicular to the substrate, such high capacity after long cycles remains remarkable. The Si/C nanocomposites prepared by the TPR shows comparable[23, 28] or even slightly better[19-21, 24-27] lithium storage performance compared to these obtained by elaborate multistep deposition/surface modification processes. The TPR is one of the very few approaches capable of preparing Si/C nanocomposites in one single step. The high performance of the TPR prepared Si/C nanocomposites suggests that when formation of SiC is eliminated, plasma reactions are very promising for preparing Si/C nanocomposites as lithium ion battery anodes.

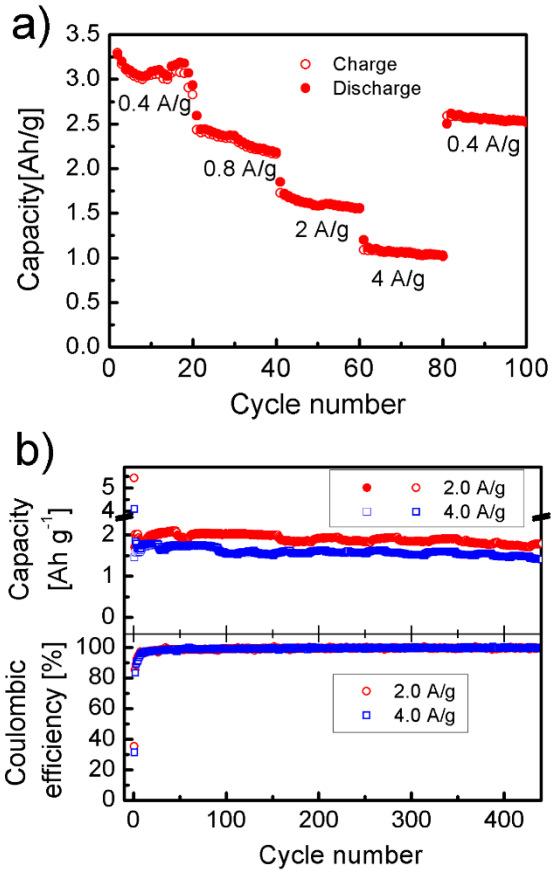

Figure 6 Cyclic performance of the Si/C-graphite sample with 10 wt% carbon in a half cell. (a) At different charge/discharge current density and (b) Capacity (the upper panel) and Columbic efficiency (the lower panel) at current density of 2.0 and 4.0 $A{\cdot}g^{-1}$. The capacity is based on all the materials on the current collector.

Conclusions

In conclusion, using the tandem plasma reaction method, we have prepared amorphous Si/C nanocomposites with very homogeneous distribution of the two components. The Si/C nanocomposites retain high capacity of 1760 and 1460 $mAh{\cdot}g^{-1}$ after more than 400 cycles at current density of 2.0 and 4.0 $A{\cdot}g^{-1}$, respectively. A key challenge in the plasma reaction is to inhibit SiC formation when both reactive Si and C species are present. This is achieved by using graphite as the carbon source, which effectively reduces the density of reactive carbon species in the plasma. We demonstrate that in a reactive medium such as plasma, unwanted compound formation can be supressed by using a less reactive precursor. This result will advance the preparation of carbon based binary nanocomposites by plasma reactions.

Acknowledgements

The authors acknowledge the financial support from the National Science Foundation of China (No. 21101007, U1201241, 11375020 and 51431001).

Notes and references

[a] Beijing National Laboratory for Molecular Sciences (BNLMS), (The State Key Laboratory of Rare Earth Materials Chemistry and Applications), College of Chemistry and Molecular Engineering, Peking University, Beijing 100871, China.
[b] Academy for Advanced Interdisciplinary Studies, Peking University, Beijing 100871, China.
[c] BTR New Energy Materials Inc. High Tech Industrial Park, Xitian, Gongming Town, Guangming New District, Shenzhen, China
[d] State Grid Smart Grid Research Institute, Beijing, China 102211
* Corresponding authors: zhengjie@pku.edu.cn, xgli@pku.edu.cn

Electronic Supplementary Information (ESI) available: [A cross section SEM image, EDS spectrum, CV curves and voltage-capacity curves of the Si/C-graphite sample; a TEM image, elemental mapping and CV curves of the Si/C-CH_4 sample]. See DOI: 10.1039/b000000x/

1. J. M. Tarascon; M. Armand, *Nature* **2001,** *414*, 359.
2. M. T. McDowell; S. W. Lee; W. D. Nix; Y. Cui, *Adv. Mater.* **2013,** *25*, 4966.
3. H. Wu; Y. Cui, *Nano Today* **2012,** *7*, 414.
4. J. P. Maranchi; A. F. Hepp; P. N. Kumta, *Electrochem. Solid State Lett.***2003,** *6*, A198.
5. T. Takamura; S. Ohara; M. Uehara; J. Suzuki; K. Sekine, *J. Power Sources* **2004,** *129*, 96.
6. L. B. Chen; J. Y. Xie; H. C. Yu; T. H. Wang, *J. Appl. Electrochem.* **2009,** *39*, 1157.
7. X. Xiao; P. Liu; M. W. Verbrugge; H. Haftbaradaran; H. Gao, *J. Power Sources* **2011,** *196*, 1409.
8. J. Yang; R. C. de Guzman; S. O. Salley; K. Y. S. Ng; B.-H. Chen; M. M. C. Cheng, *J. Power Sources* **2014,** *269*, 520.
9. P. R. Abel; Y. M. Lin; H. Celio; A. Heller; C. B. Mullins, *ACS Nano* **2012,** *6*, 2506.
10. C. Yu; X. Li; T. Ma; J. Rong; R. Zhang; J. Shaffer; Y. An; Q. Liu; B. Wei; H. Jiang, *Adv. Energy Mater.***2012,** *2*, 68.
11. N. Suzuki; R. B. Cervera; T. Ohnishi; K. Takada, *J. Power Sources* **2013,** *231*, 186.
12. S. Guo; H. Li; H. Bai; Z. Tao; J. Chen, *J. Power Sources* **2014,** *248*, 1141.
13. W. Li; R. Yang; X. Wang; T. Wang; J. Zheng; X. Li, *J. Power Sources* **2013,** *221*, 242.
14. Y. Tong; Z. Xu; C. Liu; G. A. Zhang; J. Wang; Z. G. Wu, *J. Power Sources* **2014,** *247*, 78.
15. M. K. Datta; J. Maranchi; S. J. Chung; R. Epur; K. Kadakia; P. Jampani; P. N. Kumta, *Electrochim. Acta* **2011,** *56*, 4717.
16. H. Li; H. Zhou, *Chem. Comm.* **2012,** *48*, 1201.
17. X. L. Wu; Y. G. Guo; L. J. Wan, *Chem. Asian J.* **2013,** *8*, 1948.
18. B. Liang; Y. Liu; Y. Xu, *J. Power Sources* **2014,** *267*, 469.
19. S. H. Ng; J. Z. Wang; D. Wexler; K. Konstantinov; Z. P. Guo; H. K. Liu, *Angew. Chem. Int. Ed.* **2006,** *45*, 6896.
20. H. Kim; J. Cho, *Nano Lett.* **2008,** *8*, 3688.
21. Y. S. Hu; R. Demir-Cakan; M. M. Titirici; J. O. Muller; R. Schlogl; M. Antonietti; J. Maier, *Angew. Chem. Int. Ed.* **2008,** *47*, 1645.
22. L. Xue; K. Fu; Y. Li; G. Xu; Y. Lu; S. Zhang; O. Toprakci; X. Zhang, *Nano Energy* **2013,** *2*, 361.
23. H. Wu; G. Yu; L. Pan; N. Liu; M. T. McDowell; Z. Bao; Y. Cui, *Nat. Comm.* **2013,** *4*.
24. X. Zhou; Y. X. Yin; L. J. Wan; Y. G. Guo, *Adv. Energy Mater.* **2012,** *2*, 1086.
25. L. Ji; X. Zhang, *Energy Environmental Sci.* **2010,** *3*, 124.
26. L. F. Cui; Y. Yang; C.-M. Hsu; Y. Cui, *Nano Lett.* **2009,** *9*, 3370.
27. A. Magasinski; P. Dixon; B. Hertzberg; A. Kvit; J. Ayala; G. Yushin, *Nat. Mater.* **2010,** *9*, 353.
28. X. Wang; L. Sun; R. Agung Susantyoko; Y. Fan; Q. Zhang, *Nano Energy* **2014,** *8*, 71.
29. H. Kim; M. Seo; M. H. Park; J. Cho, *Angew. Chem. Int. Ed.* **2010,** *49*, 2146.
30. J. K. Yoo; J. Kim; Y. S. Jung; K. Kang, *Adv. Mater.* **2012,** *24*, 5452.
31. J. Zheng; R. Yang; L. Xie; J. L. Qu; Y. Liu; X. G. Li, *Adv. Mater.* **2010,** *22*, 1451.
32. C. M. Hollabaugh; D. E. Hull; L. R. Newkirk; J. J. Petrovic, *J. Mater. Sci.* **1983,** *18*, 3190.
33. T. Rajagopalan; X. Wang; B. Lahlouh; C. Ramkumar; P. Dutta; S. Gangopadhyay, *J. Appl. Phys.* **2003,** *94*, 5252.
34. R. Hu; W. Sun; Y. Chen; M. Zeng; M. Zhu, *J. Mater. Chem. A* **2014,** *2*, 9118.
35. W. Sun; R. Hu; H. Liu; M. Zeng; L. Yang; H. Wang; M. Zhu, *J. Power Sources* **2014,** *268*, 610.
36. W. Li; R. Yang; J. Zheng; X. G. Li, *Nano Energy* **2013,** *2*, 1314.
37. W. Li; J. Zheng; T. K. Chen; T. Wang; X. J. Wang; X. G. Li, *Chem. Comm.* **2014,** *50*, 2052.
38. R. P. Chaukulkar; K. d. Peuter; P. Stradins; S. Pylypenko; J. P. Bell; Y. Yang; S. Agarwal, *ACS Appl. Mater. Interfaces* **2014,** *6*, 19026.
39. W. K. Choi; T. Y. Ong; L. S. Tan; F. C. Loh; K. L. Tan, *J. Appl.Phys.* **1998,** *83*, 4968.
40. C. D. Wagner; G. E. Muilenberg, *Handbook of x-ray photoelectron spectroscopy: a reference book of standard data for use in x-ray photoelectron spectroscopy*. Physical Electronics Division, Perkin-Elmer Corp.: 1979.
41. R. Pandey; M. Rérat; C. Darrigan; M. Causà, *J. Appl. Phys.* **2000,** *88*, 6462.
42. T. Cao; H. Zhang; B. Yan; W. Lu; Y. Cheng, *RSC Adv.* **2014,** *4*, 15131.
43. T. Welzel; I. Dani; F. Richter, *Plasma Sources Sci. Tech.* **2002,** *11*, 351.
44. N. Benchiheb; M. S. Aida; N. Attaf, *Mater. Sci. Eng. B* **2010,** *172*, 191.
45. M. A. Elliott; P. W. May; J. Petherbridge; S. M. Leeds; M. N. R. Ashfold; W. N. Wang, *Diamond Relat. Mater.* **2000,** *9*, 311.
46. J. Ma; M. N. R. Ashfold; Y. A. Mankelevich, *J. Appl. Phys.* **2009,** *105*, 043302.
47. H. Zhang; H. Xu, *Solid State Ionics* **2014,** *263*, 23.
48. M. Park; X. Zhang; M. Chung; G. B. Less; A. M. Sastry, *J. Power Sources* **2010,** *195*, 7904.
49. E. Hüger; L. Dörrer; J. Rahn; T. Panzner; J. Stahn; G. Lilienkamp; H. Schmidt, *Nano Lett.* **2013,** *13*, 1237.
50. J. Xie; N. Imanishi; T. Zhang; A. Hirano; Y. Takeda; O. Yamamoto, *Mater. Chem. Phys.* **2010,** *120*, 421.

